Peer reviewed version

Link to published version (if available):
10.1016/j.ijimpeng.2016.10.007

Link to publication record in Explore Bristol Research
PDF-document

University of Bristol - Explore Bristol Research
General rights

Effect of Fibre Orientation on the Low Velocity Impact Response of Thin Dyneema® Composite Laminates

Mark K. Hazzard[1]*, Stephen Hallett[1], Paul T. Curtis[1, 2, 3],

Lorenzo Iannucci[3], Richard S. Trask[4].

[1]Advanced Composites Centre for Innovation and Science, University of Bristol, Queen's Building, Bristol, BS8 1TR, UK.

[2]Defence Science and Technology Laboratory, Porton Down, Salisbury, SP4 0JQ, UK.

[3]Department of Aerospace Engineering, Imperial College London, Exhibition Road, London, SW7 2AZ, UK.

[4]Department of Mechanical Engineering, University of Bath, Bath, BA2 7AY, UK.

*Corresponding Author: mark.hazzard@bristol.ac.uk

Abstract

Ultra-high molecular weight polyethylene (UHMWPE) fibre reinforced composite materials are widely used in ballistic impact and collision scenarios due to their extremely high specific strength and stiffness. Exceptional levels of protection are provided by controlling the damage and deformation mechanisms over several length scales. In this study, the role of UHMWPE fibre architecture (cross-ply, quasi-isotropic and rotational "helicoidal" layups) is considered on the damage and deformation mechanisms arising from low velocity impacts with 150 J impact energy and clamped boundary conditions. Dyneema® panels approximately 2.2 mm thick were impacted with a fully instrumented hemi-spherical impactor at velocities of 3.38 m/s. Full field deformation of the panels was captured through digital image correlation (DIC). The results indicate that the cross-ply laminate [0°/90°] had the largest back face deflection, whilst quasi-isotropic architectures restricted and reduced the central deflection by an average of 43%. In the case of the [0°/90°] panel,

the deformation mechanisms were dominated by large amounts of in-plane shear with limited load transfer from primary fibres. Conversely, the failure of the quasi-isotropic panels were dominated by large amounts of panel buckling over various length scales. The observed mechanisms of deformation with increasing length scale were; through thickness fibre compression, fibre micro-buckling, fibre re-orientation with large matrix deformation, lamina kink band formation, and laminate buckling. The helicoidal panels showed that bend-twist and extension-twist coupling were important factors in controlling clamped boundary conditions and the laminate buckling/wrinkling shape. Further examination of the impact zone indicated that the damage mechanisms appear to be fibre orientation dependent, with quasi-isotropic laminates having up to 37.5% smaller impact damage zones compared with [0°/90°]. The experimental observations highlight the importance of fibre orientation in controlling the deformation mechanisms under dynamic impact, in particular limiting the shear deformation of Dyneema® panels.

1   Introduction

Ultra-high molecular weight polyethylene (UHMWPE) fibre composites are widely used in impact protection scenarios as they have an extremely high specific strength and stiffness, providing exceptional levels of perforation resistance [1-2]. UHMWPE fibres were developed in the 1960's by DSM and were trademarked as Dyneema[®], and are typically supplied as a composite material comprising unidirectional (UD) cross-plied [0°/90°/0°/90°] layup pre-impregnated with a thermoplastic matrix. Several publications on the ballistic impact of Dyneema[®] laminates have been reported [3–5], however the mechanisms of perforation and deformation are only just starting to be understood [6-7]. Under ballistic impact there are typically two regimes of damage and deformation, separated by a large delamination: front face penetration with local (proximal) deformation until the impactor is decelerated to a critical velocity, followed by membrane stretching (distal) after delamination. It is reported that the distal mode of deformation can absorb up to 6.5 times more energy than the proximal mode, leading to excellent efficiency in this region for cross-ply laminates [6]. In the distal mode the laminate is no longer failing locally around the projectile but instead has large amounts of panel deformation, extending to the boundary [8]. This current study focuses on the deformation mechanisms of the distal region (the second phase in an unperforated laminate) at low speed and the effect that fibre orientation has on these mechanisms.

Several high speed impact studies of UHMWPE on relatively thin laminates have been reported in the literature and a brief overview is given here. The theoretical deformation response at high speed stems from 1D Smith theory of ballistic impact on a single fibre, yarn, or strips of UD composite [9-10]. Upon transverse impact of a single fibre (1D) an axial tensile wave propagates along the fibre at constant velocity whilst a transverse wave develops at a much slower speed producing a cone like shape [11]. Progressing on from this, an elastic membrane model, which can be utilized for laminates, shows similar deformation mechanisms that can be used in 2D [12]. This supports a simplified

dimensionless parameterization, the Cuniff velocity $c*$ [1], that the ballistic limit of a laminate scales with the tensile wave speed and the mass specific tensile energy absorption of the fibre:

$$c* = \left(\sqrt{\frac{E}{\rho}} \, \frac{\sigma \varepsilon}{2\rho} \right)^{1/3} \tag{1}$$

Where E, ρ, σ, and Ɛ are the Young's modulus, density, tensile strength, and tensile failure strain of the fibre. This analysis however does not consider several effects such as the matrix properties [13], the influence of fibre orientation [14], and strain rate dependency of the fibres [8]. It has recently been shown that the layup orientation can have a large effect on not only the velocity to 50% chance of perforation (V50), but also in limiting back face deflection (BFD) [14-15]. Reducing BFD for an impact that does not cause laminate perforation is particularly important for applications such as helmets that have stringent design specifications to limit the amount of transverse deflection in order to prevent blunt trauma injuries. A rotational helicoidal fibre architecture has shown that BFD can be significantly reduced for a given impact and areal density; however typically at the expense of reducing V50 [15]. Currently there have been very few studies into low velocity impact of UHMWPE fibre composite panels, which may provide useful insight into the deformation mechanisms of varying fibre oriented laminates. In this study, a fully instrumented drop weight testing program with digital image correlation (DIC) has captured the full field deformation of the panels under impact. Optical microscopy and scanning electron microscopy (SEM) were employed to confirm the deformation mechanisms. The information should prove useful for numerical modelling techniques and also help bridge the gap between quasi-static and high-speed test regimes. The low-speed/high energy impact in the viscoelastic regime of the panels may also be of interest for civil applications such as cargo containers and protective helmets. At higher velocities, panels are expected to respond at a higher stiffness, however the mechanisms of deformation due to the fibre orientation prior to failure are similar [15].

2   Materials and Method

In this study HB25 and HB26 Dyneema® pre-preg materials, supplied by DSM, were used. HB25 and HB26 contain identical SK76 fibres with a diameter of approximately 17 μm and use the same polyetherdiol-aliphatic diisocyanate polyurethane (PADP) thermoplastic matrix; however HB25 has only a single cross ply [0°/90°] layup and HB26 contains four plies [0°/90°/0°/90°]. The pre-preg sub-laminates were cut to 200 mm squares and then stacked and hot pressed to form the laminate structure with a UD layer thickness of approximately 67 μm and a fibre volume fraction of 87% [16]. The hot press consolidation was performed in a 50 ton Hare hot press, with the time, temperature, and pressure cycle given in Fig. 1.
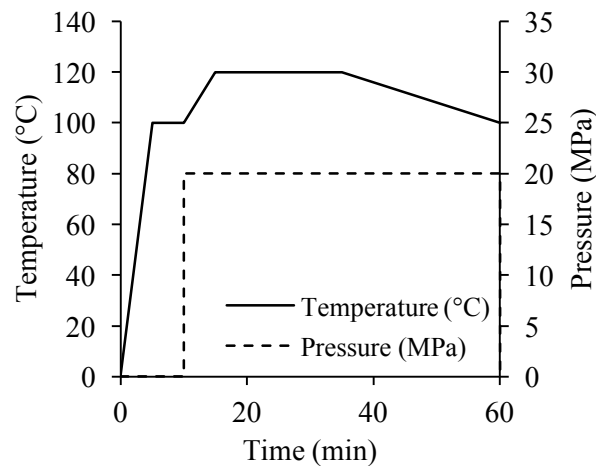

Fig. 1: Consolidation cycle used in the production of Dyneema® laminates.

2.1   Angled Ply Laminates

UD composite plies display high anisotropy between the longitudinal fibre direction (E_{11}) and the tangential non-fibre direction (E_{22}), with Dyneema® being an extreme case due to the low matrix strength and stiffness. A laminate's stiffness in a particular direction is dependent on the angle of orientation of the ply relative to a fixed axis, θ, and one can quantify the laminate stiffness through classical laminate theory at the angle of in-plane loading, φ, see Fig. 2. Dyneema® is extremely anisotropic compared structural composites such as carbon fibre epoxy as E_{11}/E_{22} can be 10 times

higher. Off axis loading of these plies therefore contributes considerably less to the in-plane stiffness for Dyneema® (Fig. 2a) compared with carbon fibre epoxy (Fig. 2b). When the laminate properties are the same in all in-plane directions, the laminate is termed quasi-isotropic. Quasi-isotropic stiffness relative to UD stiffness is lower for Dyneema® than for carbon fibre epoxy, due to the near zero contribution of the off axis stiffness's, E_{22} and G_{12}. Quasi-Isotropic laminates can have several layup orientations, and one type used here is termed helicoidal, where fibre orientation rotates through the thickness of the laminate in a consistent manner. Reducing the angle mismatch between plies, θ_n-θ_{n-1}, where θ_n is the ply angle of the nth ply through the thickness, can help reduce the tendency for composites to delaminate through minimizing the stiffness mismatch between the highly anisotropic layers of the composite material. For a helicoidal layup to be quasi-isotropic (Fig. 2), a full rotation of UD plies must occur through the thickness. Note from Fig. 2 the extreme anisotropy of Dyneema® compared with carbon fibre epoxy due to lower off-axis properties of the UD ply and that helicoidal laminates are quasi-isotropic.
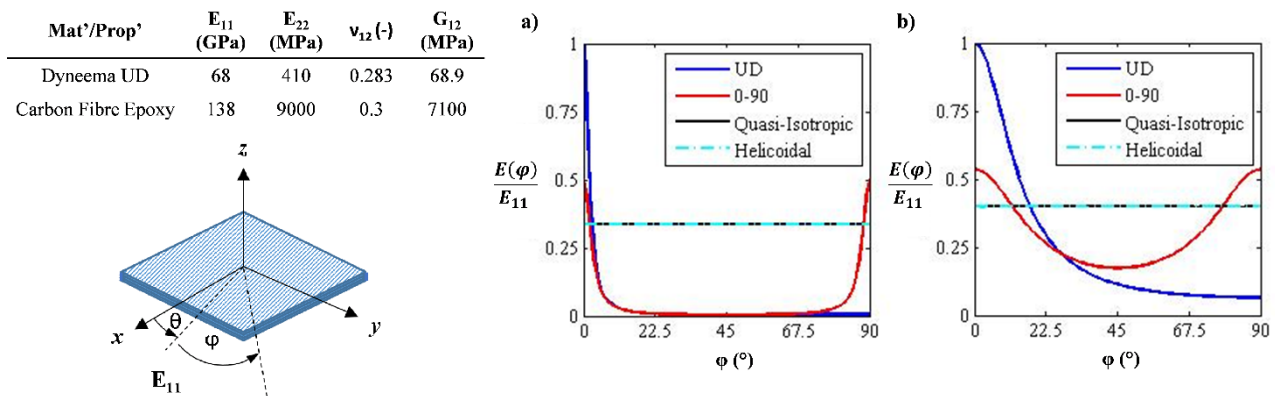

Mat'/Prop'	E_{11} (GPa)	E_{22} (MPa)	v_{12} (-)	G_{12} (MPa)
Dyneema UD	68	410	0.283	68.9
Carbon Fibre Epoxy	138	9000	0.3	7100

Fig. 2. Comparison of in-plane stiffness relative to the fibre direction UD stiffness, E_{11}, as a function of in-plane loading angle, φ, for UD, 0°/90°, helicoidal, and quasi-isotropic layups for a) Dyneema® [8] and b) carbon fibre epoxy.

2.2 Selection of Fibre Architectures

Five architectures were selected for drop weight impact testing, with three test repeats for each one. A traditional cross-ply $[0°/90°]_{16}$ layup was tested with HB25 and HB26 to compare batch performance. A quasi-isotropic layup $[[0°/90°]_2/[\pm45°]_2]_8$ using HB26 sub-laminates was also tested.

Due to the extremely low strength and stiffness properties of Dyneema® in its UD form, it is difficult to produce helicoidal laminates that use a UD pre-preg and maintain a low ply thickness. To overcome this, 3 helicoidal layups, that were also quasi-isotropic and of varying angle mismatch, were produced using HB25 sub-laminates with an angle mismatch of 22.5°, 11.25°, 5.625° named HC1, HC2, and HC3 respectively. Angled pre-preg was cut with a laser cutter to provide an accuracy of ±1°. All layups are summarized in Table 1 together with nomenclature and material type. For helicoidal laminates, the angle mismatch relates to the variation in angle between the top ply of each adjacent [0°/90°] sub-laminate (Fig. 3). All laminates are the equivalent of 32 UD plies thick.

Table 1. Test matrix of layups investigated. It is important to note that angle mismatch is between individual lamina for [0°/90°] cases and individual sub-laminates for helicoidal cases.

Nomenclature	Layup	Angle Mismatch	Material
26-090	$[(0°/90°)_2]_8$	90°	HB26
25-090	$[0°/90°]_{16}$	90°	HB25
26-QI	$[(0°/90°)_2/(\pm45)_2]_4$	90° & ±45°	HB26
25-HC1	$[(0°/90°)/(22.5/-67.5)/(45/-45)/(67.5/-22.5)]_4$	22.5°	HB25
25-HC2	$[(0°/90°)/(11.25/-78.75)/(22.5/-67.5)...(78.75/-11.25)]_2$	12.25°	HB25
25-HC3	$[(0°/90°)/(5.625/-84.375)...(84.375/-5.625)]_1$	5.625°	HB25

Laminate 25-HC2

ISOTROPIC VIEW   TOP DOWN VIEW

HB25 (0°/90°) sub-laminates

11.25°

Fig. 3. Example schematic of helicoidal layup 25-HC2 with a sub-laminate angle mismatch of 11.25°. Note that the smaller the angle mismatch of the sub-laminates, the more closely related to [0°/90°] they become.

2.3   Drop Weight Impact Setup

Drop weight impact experiments were performed using a fully instrumented Instron Dynatup 9250HV with 150 J of impact energy, a velocity of 3.38 m/s, and a mass of 26.3 kg. The velocity was confirmed through a laser gate at the point of impact, triggering the recording of force data. A custom clamping device was used to hold the panels in place during impact, with no bolting through the laminate (Fig. 4). The impactor used was a hardened steel hemisphere 20 mm in diameter which made contact at the centre of the 125 mm diameter aperture. The schematic of this setup in Fig. 4 shows the purely frictional contact between the clamp and the plate, controlled by 8 equally spaced surrounding bolts. The axial force, controlled by bolt torque, was estimated by:

$$F = \frac{T}{K.D}$$

(2)

Where T is the applied torque, K is the coefficient of friction or "nut factor" which was assumed to be 0.2 [17], D is the bolt diameter, and F is the applied axial force. All bolts were torqued twice to account for any relaxation due to any initial non-symmetric loading of the clamp. Bolts were torqued to induce a clamping pressure of 1 MPa, 2 MPa, and 4 MPa respectively for initial boundary condition investigations using 26-090 laminates. Following this all clamp pressures were maintained at 2 MPa for direct comparison between different fibre architectures.
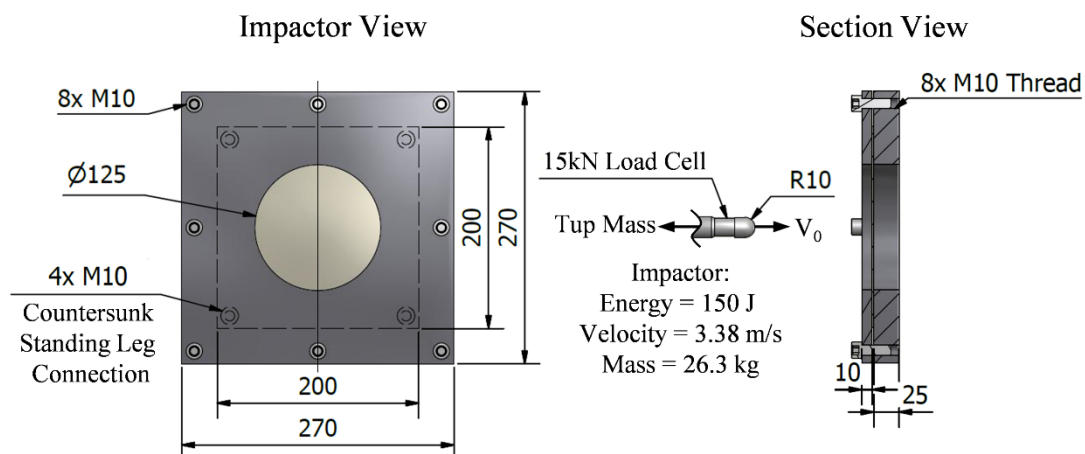

Fig. 4. Schematic of custom clamping plate highlighting the key impactor properties.

The experimental setup included two high-speed Photron Fastcam SA-Z video cameras recording in stereo via a first surface mirror in order to capture the full field back face deformation through DIC (Fig. 5). The characteristics of measurements and analyses performed through DIC are given in Table 2. A speckle pattern was manually sprayed on to the back of the Dyneema® laminates using black and white spray paint and was illuminated by 4 LED lights during testing. The first ply orientation of all laminates was 0°, which appears vertically in all DIC analyses.
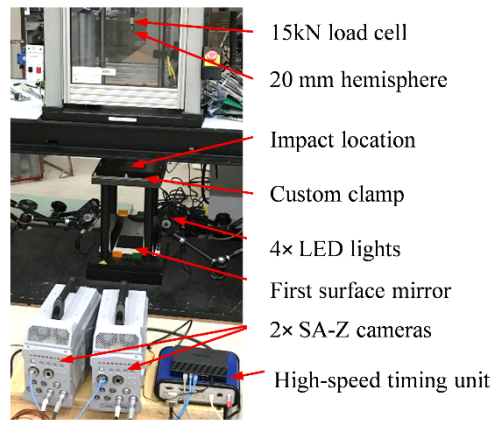

Fig. 5. Drop-weight impact tower final setup with two SA-Z high-speed cameras working in stereo to capture the full field deformation of the panels during impact.

Table 2. Stereo DIC characteristics.

Attribute	Characteristic
Camera	Photron SAZ
Lens	Tokina 100mm F2.8-22 D
Software	LaVision DaVis 8.3.0
Resolution	988 x 1032 pixels
Field of View	174 x 165 mm
Frame Rate	10 kHz
Subset Size	19 pixels
Step Size	5 pixels
Spatial Resolution	0.83944 mm
Displacement Resolution	0.76 μm
Strain Resolution	156 μƐ

3 Results and Discussion

3.1 Boundary Conditions

The BFD of the centre of the laminate was assumed to be equivalent to the measured displacement of the drop weight. BFD vs. time was investigated for the boundary pressure variations of 1 MPa, 2 MPa, and 4 MPa with a 26-090 layup (Fig. 6). The initial transverse velocity was similar for all samples, illustrated by the initial linear region, which was estimated to be equal to the impact velocity of 3.38 m/s, as measured via the laser gate upon impact. After a time of 10 ms greater deceleration started to occur, and there seemed to be no correlation between clamping pressure and BFD. Following the maximum deflection, the BFD then reduced as some spring back occurred. Here the displacement of the drop weight will likely differ from the BFD due to rebound of the impactor. The coefficient of variation of the maximum BFD for the 9 tests, 3 at each clamp pressure, was 3.8%; indicating that the deviation between laminates with different clamping pressures was small. The coefficient of friction of Dyneema$^{®}$ is extremely low which makes the material difficult to clamp effectively, with large amounts of boundary slip and pull-in where fibres in contact with the impactor (termed the 'primary fibres') reach the edge of the laminate (Fig. 7). Fibre splitting was also evident at the boundary in the regions of pull-in, however fibre failure did not occur. As clamping pressure had little effect, all further tests were performed with 2 MPa of clamping pressure.
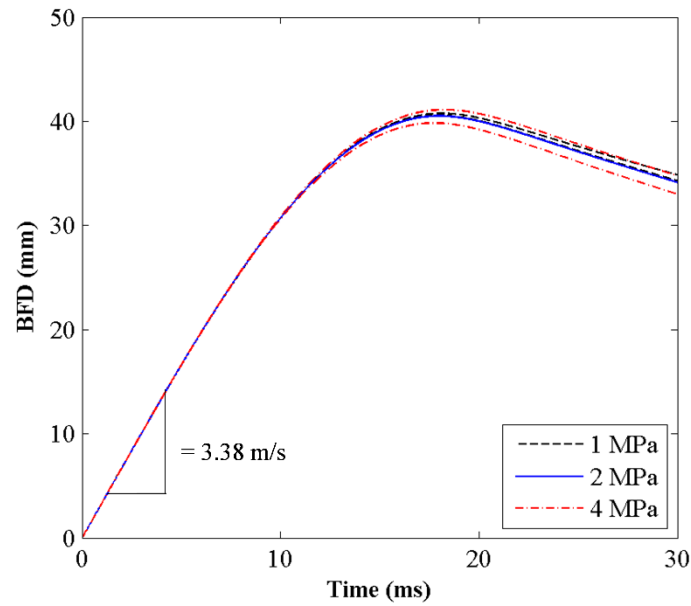
Fig. 6. Comparison of BFD with impact time of 26-090 panels with varying clamping pressures of 1 MPa, 2 MPa, and 4 MPa.
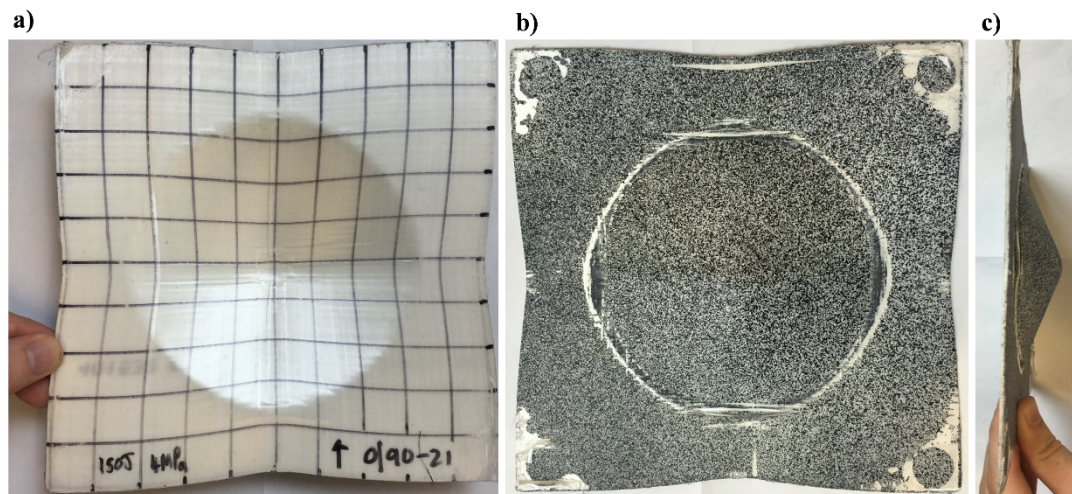

Fig. 7. 26-090 with 4MPa clamping pressure post impact a) impactor view, b) rear DIC view with speckle pattern, and c) side view. Note the pull-in located where primary fibres reach the edge of the laminate in this [0°/90°] layup.

3.2 Back Face Deflection and Contact Force

Contact force and displacement of the drop weight were continuously monitored throughout each impact and a single representative result for each layup is given in Fig. 8. Energies absorbed by the laminates, calculated through the integration of the force displacement curves, were within 4% of the

150 J impact energy as no perforation occurred. As expected 25-090 and 26-090 panels behave identically, meaning there is no difference between HB25 and HB26 sub-laminate stacks. Panel's 26-QI, 25-HC1, 25-HC2, and 25-HC3, which are all quasi-isotropic, all have a reduced BFD and a higher contact force, indicating that the impactor comes to rest over a much shorter distance. Whilst [0°/90°] layups have a relatively constant increase of BFD with increasing contact force, quasi-isotropic laminates had a sharper increase in contact force until a maximum BFD of around 7.5 mm. After this it was found that boundary slip reduced the contact force loading rate (Fig. 9). Boundary slip was caused through pull-in of the fibres at the boundary, and increases throughout the impact as friction is overcome at 7.5 mm BFD until approaching the maximum BFD where spring-back occurred. During this phase BFD starts to reduce due to the elastic portion of the deformation, however some slip increase was still seen due to boundary relaxation, particularly in the Y direction (Fig. 9). The contact force at maximum BFD has slightly higher variation for [0°/90°] laminates than for quasi-isotropic (Fig. 10). The amount of pull-in for [0°/90°] laminates was higher than for quasi-isotropic, indicating that higher boundary slip may have a large effect in the reduced contact force in [0°/90°] laminates. This is believed to be due to the large amount of in-plane shear deformation making the [0°/90°] panels harder to constrain at the boundary. This method of deformation caused the smoother force displacement curves captured in Fig. 8. 26-QI laminates on average gave the lowest BFD, the lowest amount of pull-in, and the highest contact force. Helicoidal laminates with decreasing angle mismatch tended to have a small increase in pull-in relative to the other quasi-isotropic laminates, but still lower than [0°/90°], as bend-twist and extension-twist coupling of the laminates becomes greater. All helicoidal laminates have a degree of non-symmetry about their mid-plane, which is intrinsic to the architecture. This is greatest for 25-HC3, which has increased bend-twist and extension-twist coupling. Although difficult to quantify, this is believed to promote buckling/wrinkling of the helicoidal laminates, particularly under the clamped boundary, which is clearly evident after testing (Fig. 11).
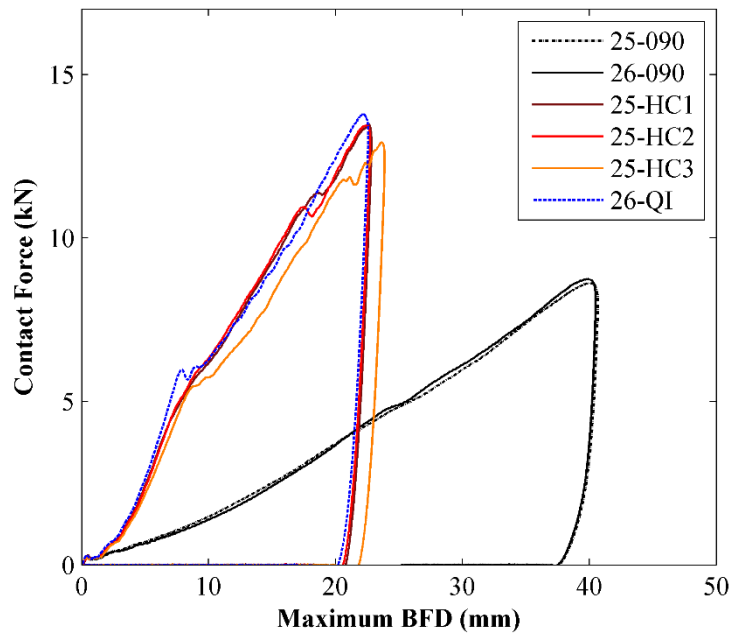
Fig. 8: Representative impacts for each laminate architecture comparing maximum BFD across the laminate with measured contact force during an impact.
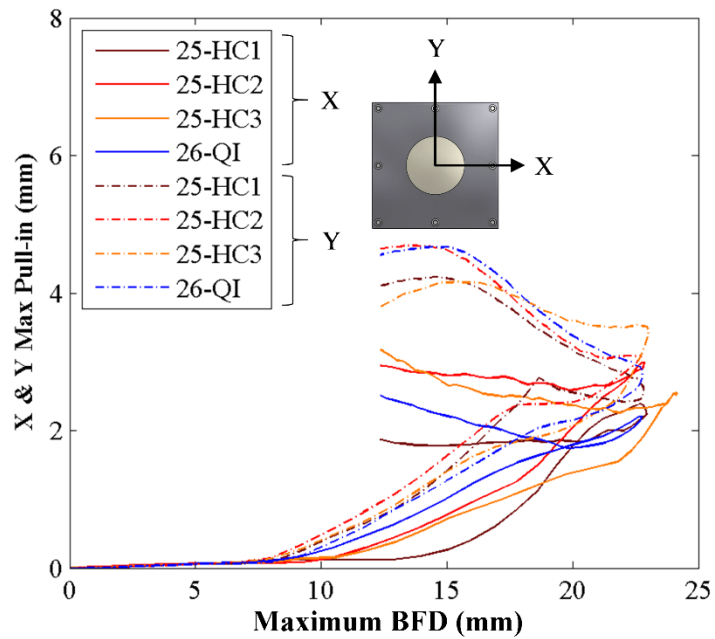

Fig. 9. Maximum BFD across the laminate with maximum X and Y pull-in (slip) from boundary measured via DIC.
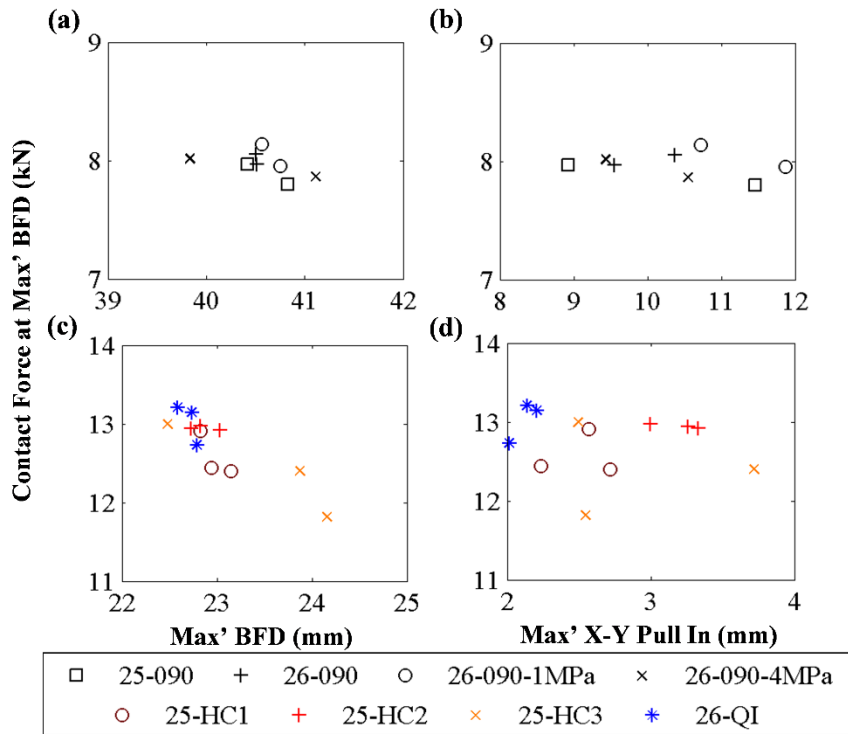
Fig. 10. Contact force at maximum deflection for a) [0°/90°] laminates with maximum measured maximum BFD, b) [0°/90°] laminates with the maximum pull-in for either the X or Y direction at maximum BFD, c) quasi-isotropic laminates with maximum BFD, and d) quasi-isotropic laminates with the maximum pull-in for either the X or Y direction at maximum BFD. Note the amount of pull-in for [0°/90°] laminates is much higher than for quasi-isotropic.
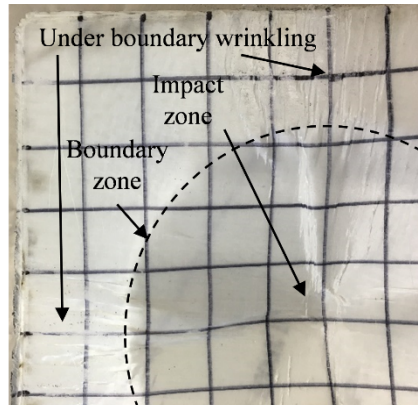

Fig. 11. A quarter view of a 25-HC3 impacted laminate. Note the wrinkling under the boundary.

3.3 Contour Map Comparison

3.3.1 0°/90° Laminates

Observations regarding the mechanisms of deformation were further analyzed through comparisons of displacement contour maps obtained from the DIC. Laminate 26-090 contour maps showed a four sided pyramid type of deformation, where large amounts of pull-in is evident (Fig. 12a). In-plane x direction strain $\mathcal{E}_{xx}$ only seems to be positive in the primary fibres, those in contact with the impactor, with strain peaking at the impact zone and approaching the failure strain of the fibres (Fig. 12b). There was also little load transfer to neighboring regions of primary fibres, with these regions actually in compression. Prior to maximum BFD, there was an increase in tension neighbouring the primary fibres as spring-back had not started to occur, however the amount of tension was still limited. Although not shown, in-plane y direction strain $\mathcal{E}_{yy}$ was similar, but positive strains were observed in the primary fibres in the *y* direction due to the [0°/90°] layup. The panels were dominated by large amounts of in-plane shear deformation, reaching strains just below $\gamma_{xy} \approx 0.1$. The largest shear deformations occurred close to the primary fibres as some tensile load is transferred via this mechanism to neighboring fibres (Fig. 12c). In these zones, grid markings on the top surface, initially positioned in a square grid following the fibre orientation, clearly show re-alignment of 90° fibres toward the point of impact (Fig. 7a). This is also known as scissoring, as the rotation of the fibres causes the angle between the [0°/90°] lamina to reduce. The in-plane shear deformation under the boundary led to an increase in the amount of boundary slip, and as this mechanism was gradual, no clear change in the rate of contact force loading can be seen in 26-090 laminates. This mechanism of boundary slip may also have been the cause for slightly higher variation in [0°/90°] laminates BFD compared with quasi-isotropic laminates (Fig. 10a-b).
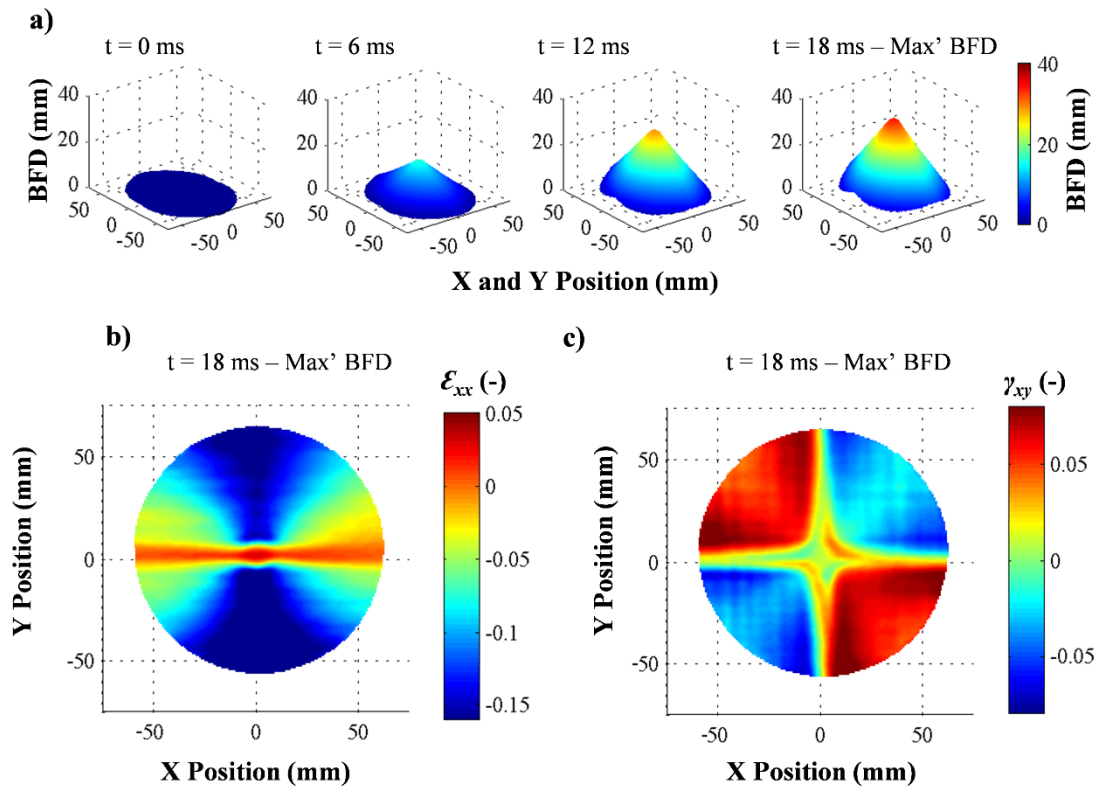
Fig. 12. Contour maps showing full field deformation of a 26-090 panel during impact. a) BFD at 0 ms, 6 ms, 12 ms, and 18 ms after impact, b) in-plane strain $\mathcal{E}_{xx}$ at maximum BFD and c) in-plane shear strain γ_{xy} at maximum BFD.

3.3.2 Quasi-isotropic and Helicoidal Laminates

Quasi-isotropic laminates deformed in a different manner from 26-090 laminates. 25-HC1, 25-HC2, 25-HC3, and 26-QI all had lower maximum back face deflections, and were dominated by wrinkling and buckling of the laminates. Here wrinkling has been used to define out of plane waviness that was under 2 mm in width that can occur throughout the laminate, and buckling is a larger global response where the buckle initiates from the impact zone and propagates to the boundary, with a typical width of 16-20 mm. Due to the scale difference, contour maps only show the large scale global buckling of 25-HC1, 25-HC2, 25-HC3 (Fig. 13), and 26-QI (Fig. 14). All showed fairly similar amounts of buckling, however the amount of wrinkling tended to increase with reduced angle mismatch. In-plane x direction strain $\mathcal{E}_{xx}$ showed a greater tensile distribution over the panel, with less of the panel being in compression. The peak strain below the impact zone was also slightly reduced (Fig. 13-14b).

Compressive zones were limited to smaller areas, particularly in the troughs of buckles, however they tended to be slightly larger in magnitude. In-plane y direction strain $\mathcal{E}_{yy}$ was similar but again oriented in the *y* direction, represented in Fig. 9. In-plane shear strain, γ_{xy}, was reduced, however large shear strains did tend to occur locally in the buckled regions, particularly in the horizontal and vertical directions, with the magnitude not varying much amongst the quasi-isotropic laminate configurations (Fig. 13-14c). From the in-plane shear contour plots it is also noticeable that with a reduction in the angle mismatch of helicoidal laminates, buckles tended to rotate from vertical positions, and following visual inspection, buckles would occasionally twist/fold over (Fig. 13c, 14c). It was thought that bend-twist and extension-twist coupling were the cause, and may have contributed to the increased slippage of these laminates under the clamped boundary.
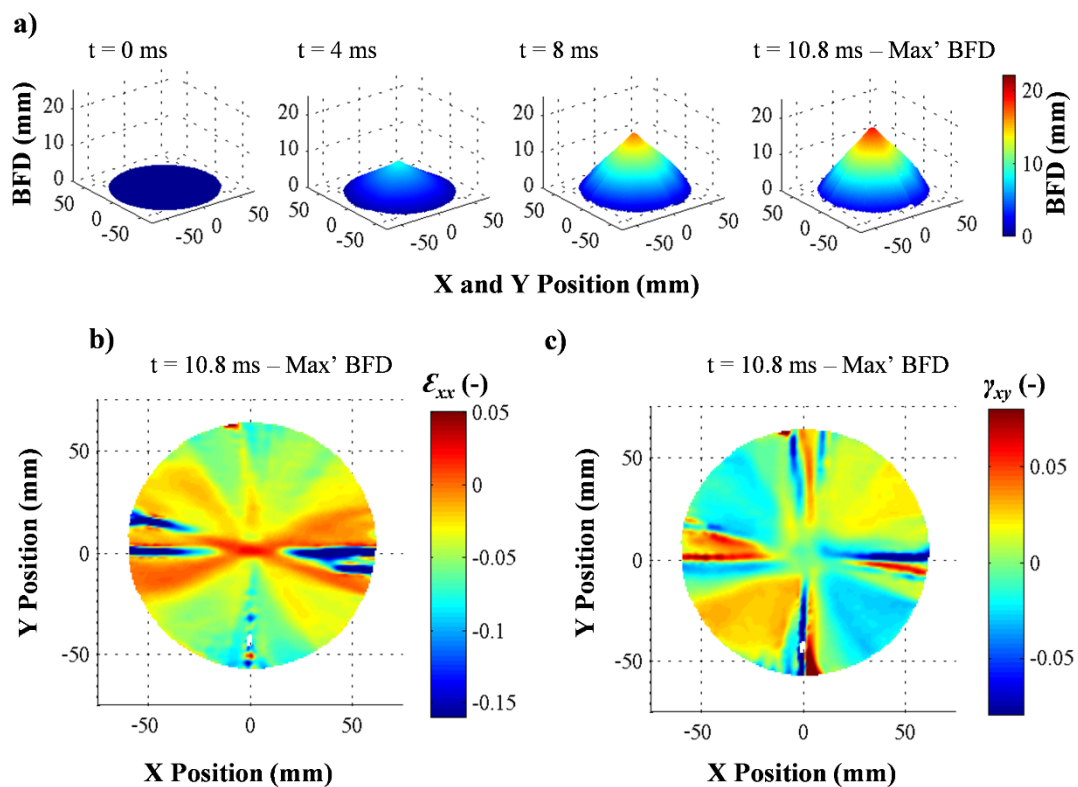

Fig. 13. Contour maps showing full field deformation of 25-HC3 panel during impact a) BFD at 0 ms, 4 ms, 8 ms, and 10.8 ms after impact, b) in-plane strain $\mathcal{E}_{xx}$ at maximum BFD and c) in-plane shear strain γ_{xy} at maximum BFD.
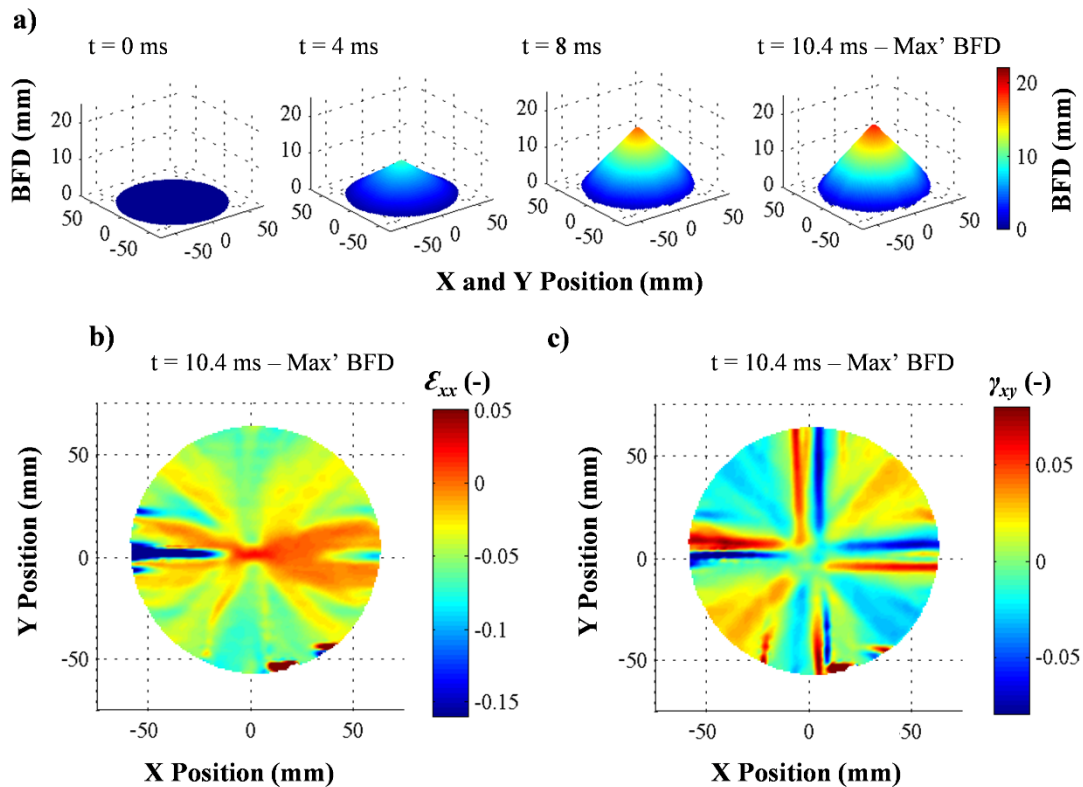
Fig. 14. Contour maps showing full field deformation of 26-QI panel during impact a) BFD at 0 ms, 4 ms, 8 ms, and 10.4 ms after impact, b) in-plane strain $\mathcal{E}_{xx}$ at maximum BFD and c) in-plane shear strain γ_{xy} at maximum BFD.

3.4 Microscopy

Fractography was performed in order to visualize the mechanisms of deformation and damage at the micro-scale through optical microscopy, surface scanning, and SEM. Dyneema[®] composites are difficult to image due to their soft nature, as mechanical cutting of the laminates tends to interfere with and amplify the original damage zones, if not undertaken with considerable care. For cross sectional microscopy, the laminates were sectioned approximately 10 mm from the zone of interest and then embedded in epoxy resin to provide additional support to the sample. Following curing at room temperature, the samples were ground down to the zone of interest and then polished for imaging. For top down imaging via SEM, a single UD layer was peeled off by hand to investigate any damage that had been caused. Note that SEM images and cross-sectional images were from two separate samples of the same layup. Surface scanning was performed on the same specimen that was

used prior to SEM and the top layer was removed prior to surface scanning. Comparisons to virgin material post-manufacture are referred to throughout, and the reader is directed to available literature for reference [4,14]. The focus in this section was on the impact zone itself (Fig. 11).

3.4.1   0°/90°

Microscopy on laminates 26-090 in the impact zone showed a large indentation approximately 12 mm in diameter with surrounding wrinkles following the [0°/90°] fibre orientation to form a square, much larger at 16 mm across (Fig. 15). From surface scanning some fibres appeared loose from the peeling back process of the top UD layer, prior to SEM. As surface scanning image composition was composed 50/50 from imagery/depth contours, pen markings on the top surface to identify large areas of deformation can be seen throughout. Directly underneath the impact, the laminate cross section was similar to that seen prior to impact, however the degree of waviness was slightly reduced (Fig. 16a). Top down SEM shows that fibres themselves appear flattened with micro-indentations from the layer above, larger in size than produced from the hot-pressing process alone (Fig. 16b). This indicates that during the impact event large compressive stresses were imparted onto the laminate under the impactor tip, leading to a combined stress state of through thickness compression and in-plane tension; with the latter indicated by in-plane strain contour mapping. Wrinkling in primary fibres particularly in the area surrounding the impact zone was prominent, and cross sectional microscopy showed symmetric kink-band formation (Fig. 17a). This was thought to be caused by in-plane compression due to Poisson contraction from primary fibres in tension, initiating micro-buckling of the fibres followed by kink-band formation at the ply level leading to wrinkling of the laminate. Surrounding the kink-band, 90° fibres running perpendicular to the wrinkle re-aligned toward the point of impact due to the low stiffness and strength, allowing large in-plane shear deformations. Due to the low shear strength of the PAPD matrix material combined with the ability of UHMWPE fibres

to bend, the matrix material becomes highly deformed and the fibres can rotate toward the point of loading.
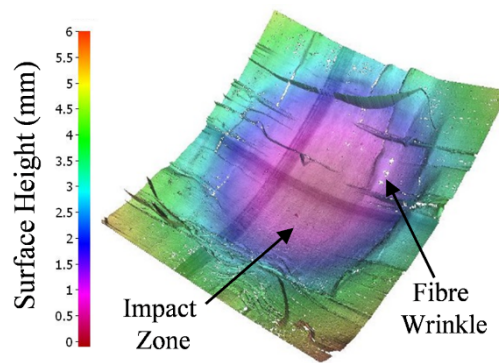

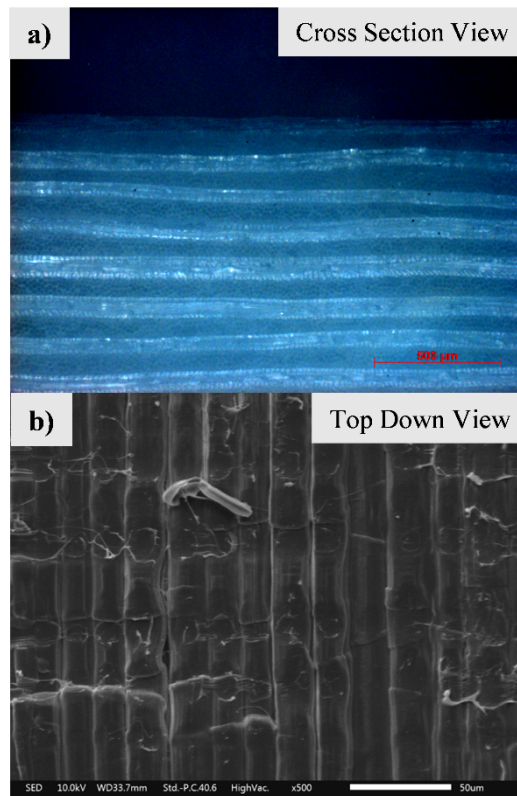**Fig. 15.** Surface scan of a 26-090 specimen prior to SEM imaging.

Fig. 16. Centre of the impact zone of a 26-090 a) cross sectional optical microscopy of impact zone centre, and b) top down SEM image.
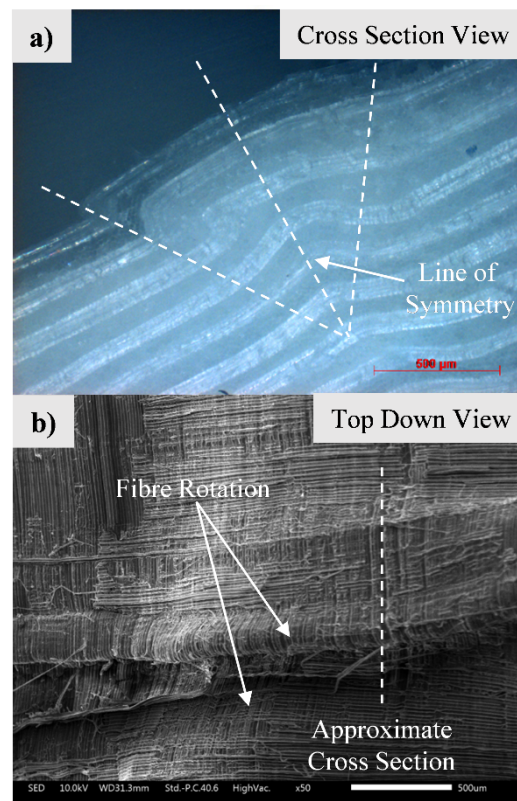
Fig. 17. Wrinkling in a 26-090 laminate a) cross sectional optical microscopy of kink-band formation, and b) top down SEM image showing wrinkling and re-aligned of fibres.

3.4.2   Quasi-Isotropic/Helicoidal

Microscopy examination of quasi-isotropic and helicoidal laminates showed different deformation and damage mechanisms. Helicoidal laminate impact zones were surrounded by circular wrinkling around the impactor, whilst 26-QI tended to have less wrinkling and more similarities to 26-090 laminates (Fig. 18a-c). The size of the damage zone compared with 26-090 laminates was also reduced by 37.5% to approximately 10 mm across and the indentation depth reduced compared with the surrounding laminate. Cross section images highlighted the layup of the quasi-isotropic configurations, with examples 25-HC1, 25-HC3, and 26-QI provided (Fig. 18d-f). As the layup orientation departs from [0°/90°], the layers tend to become more blurred in optical microscopy and layers can become difficult to differentiate. Optical cross section microscopy of the wrinkles showed that helicoidal laminate kink band formations were no longer symmetric about a central mid-plane

given in Fig. 17, however 26-QI still appeared symmetrical (Fig. 18g-i). Top down SEM imaging also proved more difficult for quasi-isotropic laminates as the layer imaged was easily separated during the peel-off process of the layer above (Fig. 18j-l). This may have been caused by an increase in the amount of ply damage during the impact itself compared with 26-090 laminates. In the impact zone there was also clear evidence of fibre flattening, although it was more difficult to locate due to the disturbed fibres in this zone. The top down imaging of the wrinkles showed much less fibre re-orientation toward the point of impact compared with that of the 26-090 laminates. This was due to the increase in the laminate shear stiffness, and local wrinkles were caused more by micro-buckling of fibres rather than large in-plane fibre curvatures (Fig. 18j-l).
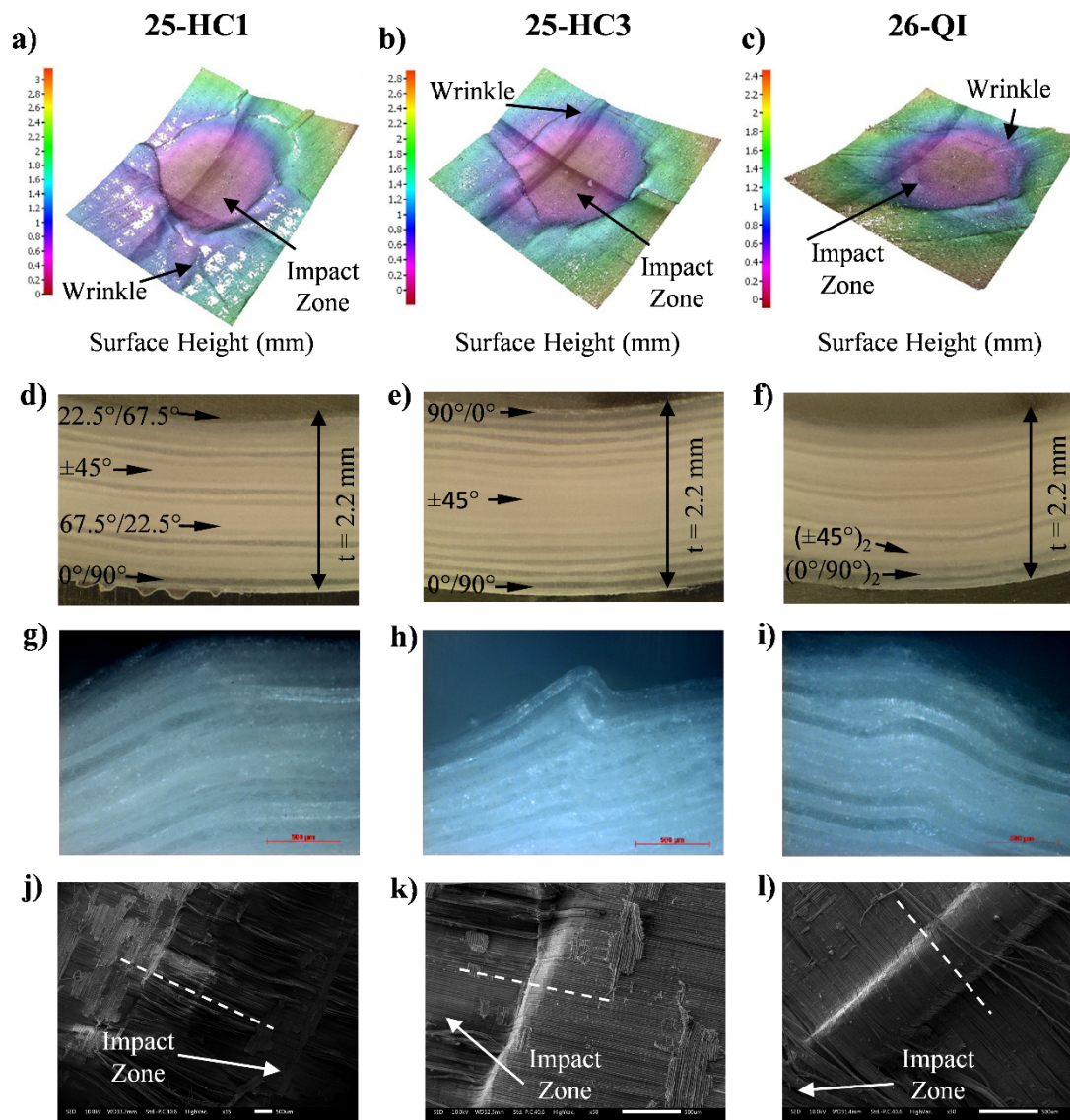
Fig. 18. Microscopy for quasi-isotropic laminates with columns representing 25-HC1, 25-HC3, and 26-QI from left to right. a-c) provide surface scans of the impact zones, d-f) cross sectional microscopy of the full laminate thickness highlighting fibre orientation, g-i) cross sectional microscopy highlighting kink-band formation that is non-symmetrical for helicoidal laminates, j-l) top down SEM images of wrinkling in the laminates with dashed line indicating approximate cross section image location.

4   Conclusion and Discussion

This study presented the low-speed impact behavior of thin Dyneema® composite laminates through impact testing at 150 J of energy with a 20 mm diameter blunt hemi-spherical impactor. A custom clamping device with a 125 mm diameter aperture was used to hold the 2.2 mm thick laminates in place during the impact event. The highly instrumented setup allowed for vast amounts of data to be

collected, with the thorough analysis of the full field deformation expected to contribute towards ongoing numerical modelling techniques. Several fibre architectures were investigated to assess the varying mechanisms of deformation, followed by microscopy to understand these processes of deformation and damage formation at the micro-scale.

The results clearly showed that quasi-isotropic laminates had on average a 43% lower maximum back face deflection compared with [0°/90°] laminates, with the time taken to maximum back face deflection also greatly reduced. The effect of angle mismatch between HB25 sub-laminates for quasi-isotropic layups was also investigated. The difference in BFD was minimal, however helicoidal laminates had slightly larger BFD with an increase in slip at the boundary. This was thought to be caused by the non-symmetrical layup, causing bend-twist and extension-twist coupling, leading to increased slip under the clamped boundary conditions due to laminate wrinkling. This observation may prove to be important in future structural design of alternate laminate architectures to minimize BFD. Varying the clamping pressure on the boundary conditions also seemed to have little effect on the maximum BFD due to the low coefficient of friction of Dyneema[®].

The resulting deformation shape for [0°/90°] panels appeared to be a four sided pyramid, controlled through large amounts of in-plane shear deformation. DIC showed that tensile strains were located in primary fibres in contact with the impactor, however load was not transferred to surrounding regions, which were often in compression. Analysis through visual inspection, optical microscopy and SEM showed that during in-plane shear deformations, large amounts of fibre re-alignment occurred. Assuming that the fibres in the primary direction were 0°, 90° fibres shifted due large in-plane shear and started to re-align toward the point of impact causing large curvatures. This was observed at a global level in the region of primary fibre transfer load to neighboring fibres, through visual inspection, as well as at a local level with wrinkling of groups of fibres, through SEM. By comparison, quasi-isotropic panels were dominated by large amounts of panel buckling that initiated from the impact zone and progressed to the boundary. DIC showed this type of deformation reduced the

distribution of in-plane shear strain throughout the panel but instead localized this to the edge of buckle regions. Similarly tensile strains were better dispersed and the peak strain beneath the impact zone appeared to be reduced. Compressive strains were confined to regions of large out of-plane buckling displacements, particularly in the troughs of buckles.

The impact zone size and shape altered depending on the layup. Surface scans showed a circular indent surrounded by an outer square of wrinkling for [0°/90°] laminates, quasi-isotropic helicoidal laminates showed circular wrinkling surrounding the impact zone, whilst the traditional [0°/90°/±45°] quasi-isotropic laminate showed a combination of the two, with less wrinkling. These observations clearly highlight how the various fibre orientations influence the local damage mechanisms. All laminates showed fibre compressive damage under SEM through fibre crushing, and cross section imaging of buckled regions showed an increase in the non-symmetry of wrinkles with higher bend-twist and extension twist-coupling.

These observations show that fibre orientation is important for controlling the deformation mechanisms under impact, in particular limiting the in-plane shear deformation of Dyneema$^{®}$ panels. Helicoidal fibre orientations showed a small difference in back face deflection compared with traditional [0°/90°/±45°] quasi-isotropic layups, thought to be due to the non-symmetrical layup which allowed for increased bend-twist and extension twist coupling, causing slip under the boundary clamp. In the future, further investigation of these laminate architectures is required in order to determine other failure mechanisms, particularly for front face armour design in the local penetration (proximal) zone where the membrane stretching mode is no longer the dominant mode of deformation. This work will also be utilized in future for the verification and validation of numerical modelling techniques.

5 Acknowledgements

6 References

[[1] P.M. Cunniff. Dimensionless parameters for optimization of textile-based body armor systems, in *Proceedings of the 18th International Symposium on Ballistics*, 1999, pp. 1303–10.

[2] H. van der Werff, U. Heisserer. High-performance ballistic fibers: ultra-high molecular weight polyethylene (UHMWPE), in *Advanced Fibrous Composite Materials for Ballistic Protection*, Woodhead Publishing, 2016, pp. 71–107.

[3] M. Iremonger. Polyethylene composites for protection against high velocity small arms bullets, in *Proceedings of the 18th International Symposium of ballistics*, 1999, pp. 15–19.

[4] U. Heisserer, H. Van der Werff, J. Hendrix. Ballistic depth of penetration studies in Dyneema® composites, in *27th International Symposium on Ballistics*, Freiberg, 2013.

[5] L. Nguyen, S. Ryan, S. Cimpoeru. The effect of target thickness on the ballistic performance of ultra high molecular weight polyethylene composite, *International Journal of Impact Engineering*, vol. 75, pp. 174–183, 2015.

[6] K. Karthikeyan, B. Russell. Polyethylene ballistic laminates: Failure mechanics and interface effect, *Materials & Design*, no. 63, pp. 115–125, 2014.

[7] M.R. O'Masta. Mechanisms of Dynamic Deformation and Failure in Ultra- High Molecular Weight Polyethylene Fiber-Polymer Matrix Composites, University of Virginia, 2014.

[8] B.P. Russell, K. Karthikeyan, V.S. Deshpande, N.A. Fleck. The high strain rate response of Ultra High Molecular-weight Polyethylene: From fibre to laminate, *International Journal of Impact Engineering*, vol. 60, pp. 1–9, 2013, (doi: 10.1016/j.ijimpeng.2013.03.010).

[9] J. Smith, F. McCrackin, H. Schiefer. Stress-Strain Relationships in Yarns Subjected to Rapid Impact Loading Part V: Wave Propagation in Long Textile Yarns Impacted Transversely, *Textile Research Journal*, 1958.

[10] S. Chocron, N. King, R. Bigger, J. Walker, H. van der Werff, U. Heisserer. Impacts and Waves in Dyneema HB80 Strips and Laminates, *Journal of Applied Mechanics*, vol. 80, no. 3, 2013, (doi: 10.1115/1.4023349).

[11]   B.A. Cheeseman, T.A. Bogetti. Ballistic impact into fabric and compliant composite laminates, *Composite Structures*, vol. 61, no. 1, pp. 161–173, 2003.

[12]   S.L. Phoenix, P. Porwal. A new membrane model for the ballistic impact response and V50 performance of multi-ply fibrous systems, *International Journal of Solids and Structures*, no. 40 (24), pp. 6723–6765, 2003.

[13]   K. Karthikeyan, B.P. Russell, N.A. Fleck, H.N.G. Wadley, V.S. Deshpande. The effect of shear strength on the ballistic response of laminated composite plates, *European Journal of Mechanics - A/Solids*, vol. 42, pp. 35–53, 2013, (doi: 10.1016/j.euromechsol.2013.04.002).

[14]   L. Vargas-Gonzalez, J. Gurganus. Hybridized composite architecture for mitigation of non-penetrating ballistic trauma, *International Journal of Impact Engineering*, vol. 86, pp. 295–306, 2015.

[15]   K. Karthikeyan, S. Kazemahvazi, B. Russell. Optimal fibre architecture of soft-matrix ballistic laminates, *International Journal of Impact Engineering*, no. 88, pp. 227–237, 2016.

[16]   M.K. Hazzard, P.T. Curtis, L. Iannucci, S. Hallett, R. Trask. An Investigation of the in-plane performance of ultra-high molecular weight polyethylene fibre composites, in *International Conference of Composite Materials*, Copenhagen, 2015, no. July, pp. 19–24.

[17]   O. Nixon-Pearson, S. Hallett. An experimental investigation into quasi-static and fatigue damage development in bolted-hole specimens, *Composites Part B: Engineering*, vol. 77, pp. 462–473, 2015.